Water Research 229 (2023) 119452

Contents lists available at ScienceDirect

Water Research

journal homepage: www.elsevier.com/locate/watres

Mitigation of ultrafiltration membrane fouling by a simulated sunlight-peroxymonosulfate system with the assistance of irradiated NOM

Dong Li [a,b], Haiyang He [b], Jialin Jia [b,c,*], Wei Shi [b,d], Feng Yin [a], Jianghua Yu [a], Mindong Chen [a], Jun Ma [b,*]

[a] Collaborative Innovation Center of Atmospheric Environment and Equipment Technology, Jiangsu Key Laboratory of Atmospheric Environment Monitoring and Pollution Control, School of Environmental Science and Engineering, Nanjing University of Information Science & Technology, Nanjing 210044, People's Republic of China

[b] State Key Laboratory of Urban Water Resources and Environment, School of Environment, Harbin Institute of Technology, Harbin 150090, People's Republic of China

[c] College of Environment, Hohai University, Nanjing 210098, People's Republic of China

[d] China Everbright Water Limited, Shenzhen 518033, People's Republic of China

ARTICLE INFO

Keywords:
Peroxymonosulfate
Sunlight
Ultrafiltration
Membrane fouling
Natural organic matter
Surface water treatment

ABSTRACT

Oxidation pretreatments prior to ultrafiltration are hindered by the need for energy input and sludge disposal. Herein, a simulated sunlight-induced natural organic matter (NOM) for peroxymonosulfate (PMS) activation was used as pretreatment to alleviate ultrafiltration membrane fouling caused by NOM itself in the Songhua River water. When light intensity was over 100 mW/cm^2, the pretreatment removed NOM effectively, characterized with UV_{254}, dissolved organic carbon (DOC) and maximum fluorescent intensity (F_{max}), and improved filtration flux. At 200 mW/cm^2 light intensity and 0.5 mM PMS, 57.5% of UV_{254} and 18.5% of DOC were removed, and humic-like fluorescent component was degraded by 84%-94% while ~60% for protein-like substance. Membrane flux was increased by 94%, and reversible and irreversible fouling resistances were reduced by 62.4% and 51.9%, respectively. Both total fouling index (TFI) and hydraulic irreversible fouling index (HIFI) were moderately correlated with the DOC, whereas they prominently correlated with the UV_{254} and the F_{maxs} of all fluorescence components, which could be served as key indicators to predict and control membrane fouling. Mathematical modeling showed that the pretreatment alleviated the fouling in the membrane pores and cake layer. The simulated sunlight-induced NOM (^{3}NOM* and e^-_{aq}) could activate PMS to form active species, which enabled to oxidize high molecular weight (MW) substances and mineralize low MW compounds in NOM as well as hinder their linking with inorganic cations, thereby reducing organic and inorganic membrane fouling simultaneously. This study may provide a new strategy for decentralized potable water treatment, especially in a single household or community.

1. Introduction

Ultrafiltration is extensively used in drinking water purification to meet the requirements of high-quality drinking water (Peter-Varbanets et al., 2009; Prézélus et al., 2021; Yu et al., 2020). The principal advantages of ultrafiltration over traditional treatment technologies are the complete removal of pathogens, stable water quality, and small footprint (Wang et al., 2020). Nevertheless, membrane fouling is a major obstacle to the efficient operation of the ultrafiltration process (Howe and Clark, 2002). Fouling impacts negatively the permeable flux of the membrane and increases operation and maintenance costs, which results in low efficiency and poor economy of ultrafiltration application (Wang et al., 2020; Zhao et al., 2018). Membrane fouling is unavoidable, so pretreatments are usually taken to minimize its adverse effect on water treatment (Gao et al., 2011; Peters et al., 2021; Yu and Graham, 2015).

Oxidation pretreatments prior to ultrafiltration are widely applied for the removal of organic substances to resist organic membrane fouling (Cheng et al., 2017b; Guo et al., 2020; Lin et al., 2013; Ma et al., 2018). Persulfate (peroxydisulfate (PDS) or peroxymonosulfate (PMS)), a common oxidant, is susceptible to activation to generate multiple active species, including sulfate radicals ($SO_4^{\bullet-}$), hydroxyl radicals (•OH), or

* Corresponding authors at: State Key Laboratory of Urban Water Resources and Environment, School of Environment, Harbin Institute of Technology, Harbin 150090, People's Republic of China.

E-mail addresses: huaiqiu1234@126.com (J. Jia), majun@hit.edu.cn (J. Ma).

https://doi.org/10.1016/j.watres.2022.119452
Received 17 September 2022; Received in revised form 18 November 2022; Accepted 2 December 2022
Available online 3 December 2022

singlet oxygen ($^1O_2$) (Gao et al., 2018). Especially, $SO_4^{\bullet-}$ and •OH with high oxidation potentials (2.5-3.1 and 1.9-2.7 V, respectively) enable non-selectivity to oxidize various organic compounds (Tian et al., 2022; Yang et al., 2015). The pretreatments with persulfate activation are frequently performed to mitigate membrane fouling and improve filtration flux (Cheng et al., 2018; Wan et al., 2019). When PMS is activated with Fe^{2+}, $SO_4^{\bullet-}$ oxidation and Fe^{3+} coagulation together remove substantial organics, resulting in increases in the quantity of the produced water and fouling reversibility (Cheng et al., 2017a; Cheng et al., 2017b). Ultraviolet-activated persulfate pre-oxidation achieves 58% of NOM mineralization and retards 75% of irreversible fouling during ultrafiltration of surface water (Tian et al., 2018). In other studies, heat and sunlight(100 mW/cm^2, 1-sun)-heat can activate PDS to degrade organic matter and then achieve recovery of water flux and reduction of transmembrane pressure, respectively (Guo et al., 2020; Guo et al., 2021). Despite demonstrating membrane fouling alleviation, the need for sludge disposal (such as ferric flocs) and energy input hinder the deployment of these approaches in large-scale applications.

The NOM contains humic substance (HS) and dissolved organic matter (DOM), both of which are photosensitizers (Pan et al., 2018; Wang et al., 2018). Studies reported that direct photolysis of them in water leads to the generation of reactive intermediates, including •OH, $^1O_2$, hydrated electrons (e_{aq}^-), and triplet excited state of HS/DOM/NOM (^{3}HS*/^{3}DOM*/^{3}NOM*) (Chen et al., 2009; Wang et al., 2018; Zhang et al., 2014). Of these intermediates, e_{aq}^- and ^{3}HS*/^{3}DOM*/^{3}NOM* can serve as activators to activate PMS to produce more active species. Jia et al. (2020) reported that activation of PMS with irradiated humic acid by visible light degraded both humic acid itself and bisphenol A. Nie et al. (2022) found that ^{3}DOM* is capable of reacting with PMS in a high rate constant (approximately 4×10^8 M^{-1} s^{-1}) to form $SO_4^{\bullet-}$. Importantly, NOM has been identified as the main foulant that causes membrane fouling in the ultrafiltration treatment of drinking water, especially for irreversible fouling (Howe and Clark, 2002; Lee et al., 2004; Wu et al., 2021), and solar energy is a green and sustainable resource. Hence, it is imperative to investigate the feasibility of sunlight-induced NOM for PMS activation to degrade NOM itself and alleviate ultrafiltration membrane fouling.

This study investigated the simulated sunlight-activated PMS in NOM-contained Songhua River water as a pretreatment for the ultrafiltration process. The impacts of light intensity and PMS dosage on NOM removal and membrane fouling behavior were discussed. The NOM removal was determined by organic indicators of UV_{254}, DOC, and fluorescent components. The membrane fouling was evaluated by water flux and fouling reversibility. The correlations of organic indicators with fouling indexes were established. The mechanism of membrane fouling control was elucidated by analyzing mathematical modeling of membrane fouling, MW distribution of NOM, formation of active species, and membrane characterization.

2. Materials and methods

2.1. Materials and chemicals

The surface water was collected from the Songhua River in Harbin, China. The raw water taken was pre-filtered through a 0.45 μm cellulose acetate membrane and stored at 4 °C before experiments. The main characteristics of the Songhua River water were summarized in Table S1. Potassium peroxymonosulfate ($KHSO_5{\cdot}0.5KHSO_4{\cdot}0.5K_2SO_4$, PMS) was purchased from Sigma-Aldrich (USA). The commercial flat-sheet polyethersulfone ultrafiltration membranes with an MW cutoff of 100 kDa were supplied by Shanghai Mosu Science Equipment Co., Ltd.

2.2. Experimental procedures

A schematic diagram of the experimental setup was shown in Fig. S1. The simulated sunlight-induced PMS activation was adopted to pretreat raw water before membrane filtration. The pretreatment experiments were performed in the beaker at 25 °C thermostatic water bath. The dosages of PMS were 0, 0.1, 0.3, 0.5, 0.7, and 0.9 mM, respectively. The volume of the reaction solution was 500 mL, and the solution was stirred throughout the experiment. A 300 W Xenon lamp with a Vis-REF filter (irradiating wavelength of 320–780 nm, Fig. S2) was used to provide the simulated sunlight, which was set above the beaker opening. The light intensities were 100, 150, 200, and 250 mW/cm^2 on the surface of the reaction solution, corresponding to 1-sun, 1.5-sun, 2-sun, and 2.5-sun illumination, respectively. Excess methanol and sodium thiosulfate were added immediately to quench the residual oxidants after collecting water samples. Methanol was used as a terminator for UV_{254} detection, and sodium thiosulfate was used for other indicators. The pretreatment experiments were repeated at least two times, and the average values with standard deviations were given in Figures.

The membrane filtration experiments were carried out in a dead-end ultrafiltration system (Fig. S1), which consisted of an ultrafiltration cup (MSC300, Shanghai Mosu, China), a data acquisition unit (a computer linked to an electronic balance, Denver, USA), and a high-pressure nitrogen cylinder. The new membrane was cleaned by dipping into the methanol-water mixture (volume ratio in 1:9) for 12 h to remove the organic residue on the membrane surface and in the membrane pores. The cleaned ultrafiltration membrane was placed in the ultrafiltration cup horizontally, with the filtration layer facing the influent. The filtration experiment was operated at a constant trans-membrane pressure of 0.05 MPa, and the effective filtration area was 38.5 cm^2. The permeate flux was calculated with the weight data of the effluent recorded automatically by a data acquisition unit. Each group of the experiment included the filtration of a 300 mL water sample, removal of reversible fouling, and filtration of 200 mL Milli-Q water (the detailed procedures are described in Text S1). The initial membrane flux (J_0) measured by Milli-Q water at 0.05 MPa was 132 ± 5 L/(m^2 h). After filtration, the ultrafiltration membranes were dried naturally for characterization.

2.3. Membrane fouling assessment

The resistance-in-series model based on Darcy law was used to analyze the resistance of membrane fouling. The resistance equations were listed in Text S1. The correlation of various organic indicators with membrane fouling was evaluated through the fouling index. Its detailed description was depicted in Text S2. Four typical mathematical models (complete blocking, standard blocking, intermediate blocking, and cake filtration) were usually used to analyze the ultrafiltration data and determine the mechanism of membrane fouling. The equations of the four models were shown in Table S2.

2.4. Analytical methods

The UV_{254} was determined with a UV-Vis spectrophotometer (T6, Persee, Beijing, China). The content of DOC was measured by using a total organic carbon analyzer (Multi N/C 3100, Jena, Germany). The fluorescence properties of water samples were characterized on a fluorescence spectrophotometer (F7000, Hitachi, Japan). Three-dimensional fluorescence excitation-emission matrix (EEM) was recorded at the excitation wavelengths of 200–450 nm in 5 nm intervals and emission wavelengths of 250–550 nm in 1 nm intervals. Raman scatter peaks were eliminated by subtracting the EEM of Milli-Q water from the EEM of the water sample. The parallel factor (PARAFAC) analysis using MATLAB R2014a was performed to divide fluorescence peaks into several components (Stedmon and Bro, 2008). Random assignment initial value test and split half analysis passed to prove that the PARAFAC result was correct. The concentration of each component was estimated by the F_{max} derived from the PARAFAC model. The active species were examined using an Electron Spin Resonance spectrometer

(ESR, Bruker A200). The MW distribution of NOM in water sample was detected by high-performance size exclusion chromatography (HPSEC) through a UV detector. The mobile phase was a phosphate buffer solution of pH 6.85, containing 2 mM K_2HPO_4, 2 mM KH_2PO_4, and 100 mM NaCl.

The fouling of membrane surface was observed using a scanning electron microscope (SEM, SU8010, Hitachi, Japan). Atomic force microscopy (AFM, Icon, Bruker) was utilized to observe the surface roughness of the membrane. The chemical composition and functional groups of foulants were recorded by the energy dispersive X-Ray (EDX) spectroscopy and attenuated total reflectance Fourier transform infrared spectroscopy (ATR-FTIR, Spectrum One, PerkinElmer, USA), respectively.

3. Results and discussion

3.1. NOM removal by pretreatment

3.1.1. Removals of UV_{254} and DOC

The UV_{254} and DOC content are typical indicators for characterizing NOM in surface water. Fig. 1a–d showed the removal results of UV_{254} and DOC of the Songhua River water under different light intensities and PMS concentrations. PMS pre-oxidation alone hardly removed UV_{254} and DOC in raw water. Ultrafiltration alone exhibited slight removal for both UV_{254} and DOC (Fig. S3), which was in accordance with previous reports (Guo et al., 2021; Shao et al., 2017). The slight removal was due to the interception of a small amount of organic matter by ultrafiltration membrane, while most organics could pass through the membrane pores. This part of the intercepted substance would lead to severe membrane fouling. For the simulated sunlight-induced PMS pretreatment, removal efficiencies of UV_{254} and DOC were much improved with the increase in light intensity (Fig. 1a and b). The 100 mW/cm^2 intensity induced PMS system revealed limited removals for both UV_{254} (14.2%) and DOC (1.4%). When light intensity was over 100 mW/cm^2, efficient removals of UV_{254} and DOC were observed. The removal efficiencies of UV_{254} were 40.8%, 57.5%, and 62.9% at light intensity of 150, 200, and 250 mW/cm^2 after 180 min of reaction, respectively. The removal rate of DOC increased from 7.2% to 19.2% as light intensity increased from 150 to 250 mW/cm^2. Rising light intensity might accelerate activation of PMS and formation of active species, and then enhance degradation of organic matter. However, enhancement degree of removal efficiencies for both UV_{254} and DOC was insignificant as light intensity increased from 200 to 250 mW/cm^2.

Fig. 1c and d displayed the effects of PMS dosage on UV_{254} and DOC removals. Direct simulated sunlight irradiation (200 mW/cm^2) had a slight UV_{254} removal (8.9%) but no DOC removal, which indicated that simulated sunlight alone failed to remove the NOM after 180 min irradiation significantly. The removal efficiencies of both UV_{254} and DOC were increased as increasing PMS dosage. The removal efficiencies of UV_{254} were 27.9%, 47.8%, 57.5%, 65.6%, and 70.8% at PMS dosages of 0.1, 0.3, 0.5, 0.7, and 0.9 mM, respectively. The removal efficiency of DOC increased from 2.1% to 22.3% when concentration of PMS was increased from 0.1 to 0.9 mM. In contrast, the removal efficiency of UV_{254} exceeded that of DOC, which implied that the simulated sunlight-induced PMS activation first destroyed the structure of NOM in raw water, and then mineralized it into CO_2. Hence, a faster decrease of

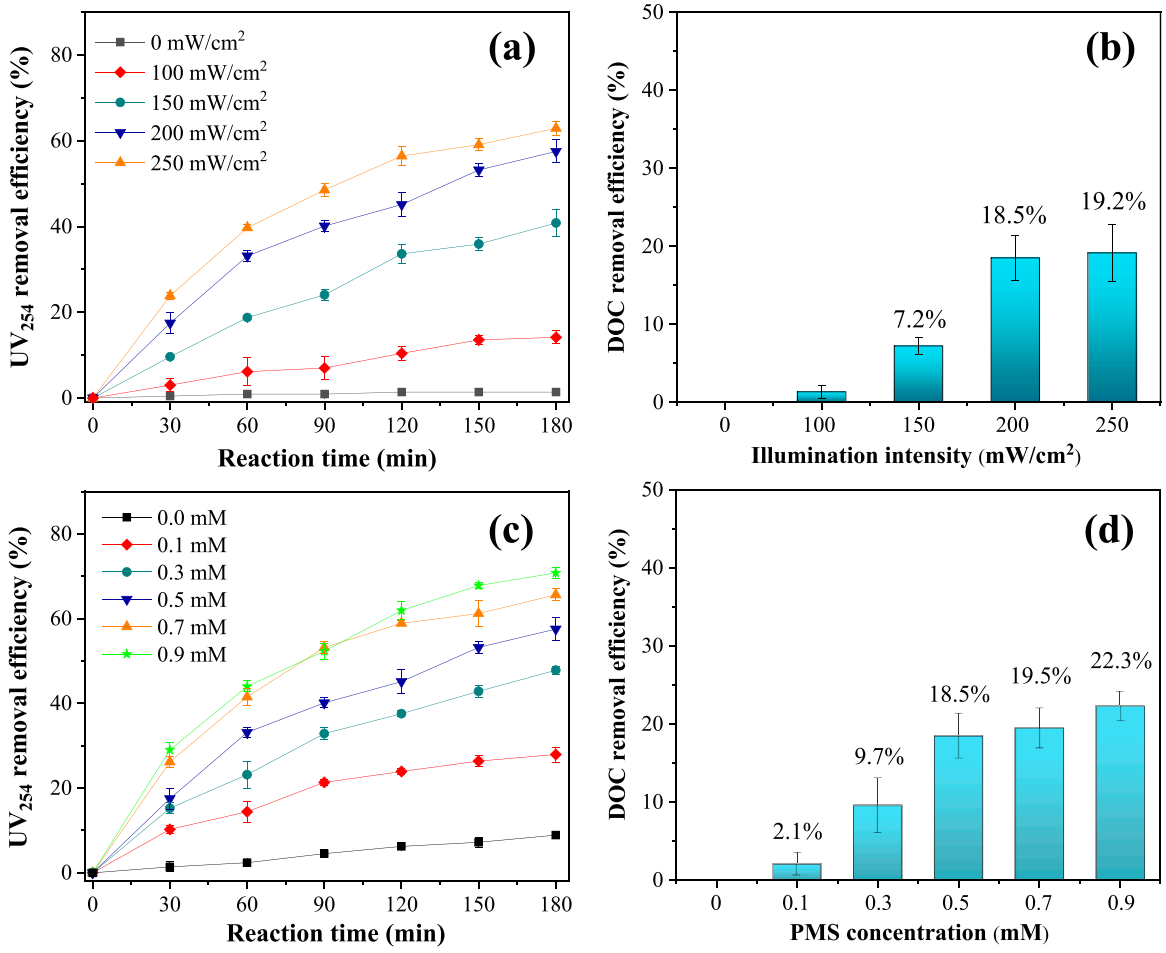

Fig. 1. Removal efficiencies of UV_{254} and DOC with the pretreatment at different light intensities (a, b; $[PMS]_0$=0.5 mM) and PMS concentrations (c, d; light intensity=200 mW/cm^2).

UV_{254} and a slower reduction of DOC occurred. Supportively, previous studies also reported that the pre-oxidation was more likely to destroy the unsaturated bonds and aromatic structures of NOM than mineralized it because the latter required more energy, thus generally leading to the more removal of UV_{254} relative to DOC (Guo et al., 2020; Guo et al., 2021; Tian et al., 2018). Nevertheless, the removal efficiency of DOC in our system was lower than that in previous systems. This was likely because the induced NOM used for PMS activation was preferentially degraded, while a small proportion of UV light in the simulated sunlight had less reactivity for PMS activation (Nie et al., 2022).

3.1.2. *Removal of fluorescent organic matter*

According to the published literature (Tian et al., 2016; Wells et al., 2022; Xing et al., 2018), NOM mainly consists of humic-like substance and protein-like matter that can be reflected by fluorescence EEM analysis. Thus, the three-dimensional fluorescence EEM of sample was recorded to further discuss the characteristic variation of NOM. The fluorescent spectrum of raw water was shown in Fig. S4, and three typical components were identified with the PARAFAC analysis. All three fluorescent components displayed a bimodal structure with the main and secondary peaks (Fig. S5). Component 1 (C1) displayed two maximum excitation wavelengths (Ex) at 240 nm and 310 nm and a broad emission wavelength (Em) in the range of 380–430 nm, which was assigned to the marine or microbial humic-like matter (Guo et al., 2020; Shao et al., 2014). Component 2 (C2, Ex/Em=270(360)/460-470 nm) represented the terrestrially derived humic-like substance (Guo et al., 2020; Shao et al., 2014). Component 3 (C3, Ex/Em=225(280)/310–320 nm) was related to the protein-like substance derived from biological generation in surface water (Guo et al., 2020; Shao et al., 2014).

The variations in the removal efficiency of fluorescent components were shown in Fig. 2. The PMS oxidation alone could hardly remove the C1, C2, and C3 (Fig. 2a). Interestingly, the sunlight-induced PMS activation revealed apparent removals for both C1 and C2 components at a light intensity of 100 mW/cm^2, which implied that 1-sun illumination could display efficient removals for C1 and C2. This was slightly different from the removal results of UV_{254} and DOC (low removal of UV_{254} and no removal of DOC at 100 mW/cm^2), indicating that C1 and C2 humic-like substances were more susceptible to degradation in comparison with UV_{254} and DOC. Similar results were also found in other pre-oxidation systems (Guo et al., 2020; Guo et al., 2021; Tian et al., 2018). A probable interpretation was that the groups with fluorescent components on humic-like matters were preferentially destroyed/degraded. When light intensity was over 100 mW/cm^2, excellent removals of C1 and C2 components were found. Similar to removals of UV_{254} and DOC, as light intensity increased from 200 to 250 mW/cm^2, a slight enhancement of C1 and C2 removals was observed. This further showed that more energy input did not remove more organics to some extent. Efficient removal of C3 was observed at light intensity over 100 mW/cm^2. The C3 component belonged to protein-like substance which was sensitive to solar light. The UV part in solar light spectra would destroy their internal structure resulting in denaturation. Additionally, the active species in the solution could degrade protein-like components. Considering that the Vis-REF filter provided a small amount of UV light irradiation (320–380 nm, Fig. S2), active species might be responsible for removal of C3.

As shown in Fig. 2b, 200 mW/cm^2 (2-sun) irradiation alone showed the measurable removal of fluorescent components. With increased PMS dosage, the pretreatment became more effective for removing C1 and C2 components. Most fluorescent matters were degraded within 180 min, and removal efficiency gradually reached a plateau in the following reaction when PMS was used at a higher dosage (0.5–0.9 mM). The difference in removal efficiency was diminished at higher PMS dosages. In addition, regardless of light intensity and PMS dosage, C2 was the most readily removed component, followed by C1, which conformed to the previous conclusion that preferential removal of terrestrial organic substances over microbial matters (Chen et al., 2017). When 0.1 mM PMS was added, the C3 component was obviously removed, and increasing PMS dosage clearly boosted C3 removal, which supported that the removal of C3 was mainly attributed to the oxidation of active species. The final removal efficiencies of C1 and C2 were over 87% and 99% at a PMS dosage of 0.9 mM, respectively, and nearly 72% of C3 was degraded. Strangely, C1 removal efficiency at 0.9 mM PMS was lower than that at 0.7 mM PMS, which might be interpreted with the different initial F_{max} values. It is well known that humic-like and protein-like substances are closely related to membrane fouling, which can adhere to the membrane surface or/and block the membrane pores, leading to a decrease in filtration flux (Cheng et al., 2016; Yu et al., 2020; Zularisam et al., 2007). Owing to effective removals of humic-like and protein-like matters, it was reasonable to expect that sunlight-induced PMS pretreatment could mitigate membrane fouling during ultrafiltration treatment of surface water.

3.2. *Membrane fouling control*

The flux variations during ultrafiltration of raw and pretreated water were presented in Fig. 3a and b. The membrane flux of the ultrafiltration process of raw water was improved in different levels by pretreatment with different light intensities and PMS dosages, which implied that

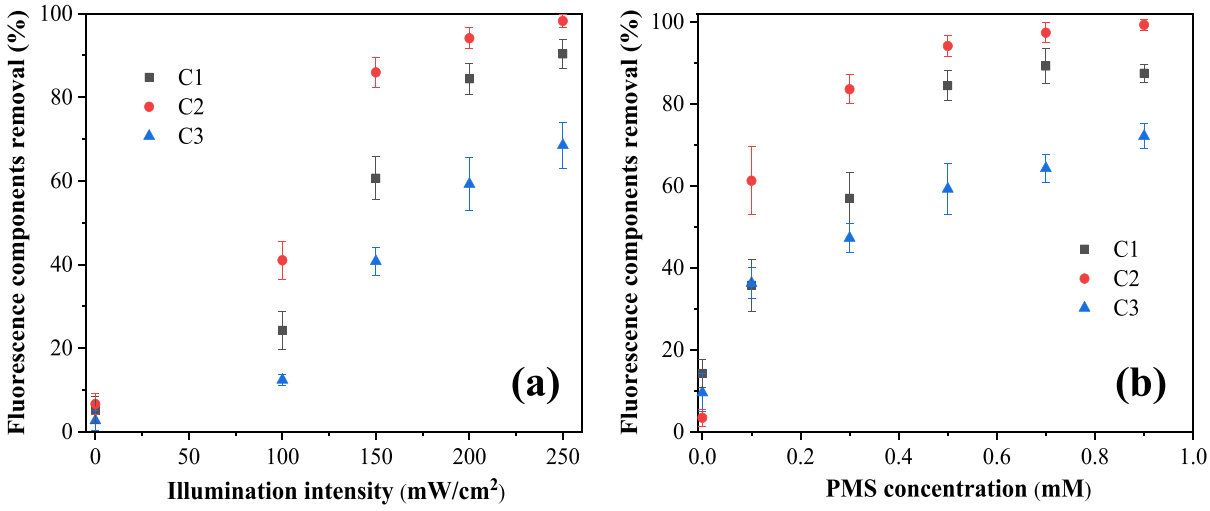

Fig. 2. Removal efficiencies of fluorescence components with the pretreatment at different light intensities (a; $[PMS]_0$=0.5 mM) and PMS concentrations (b; light intensity=200 mW/cm^2).

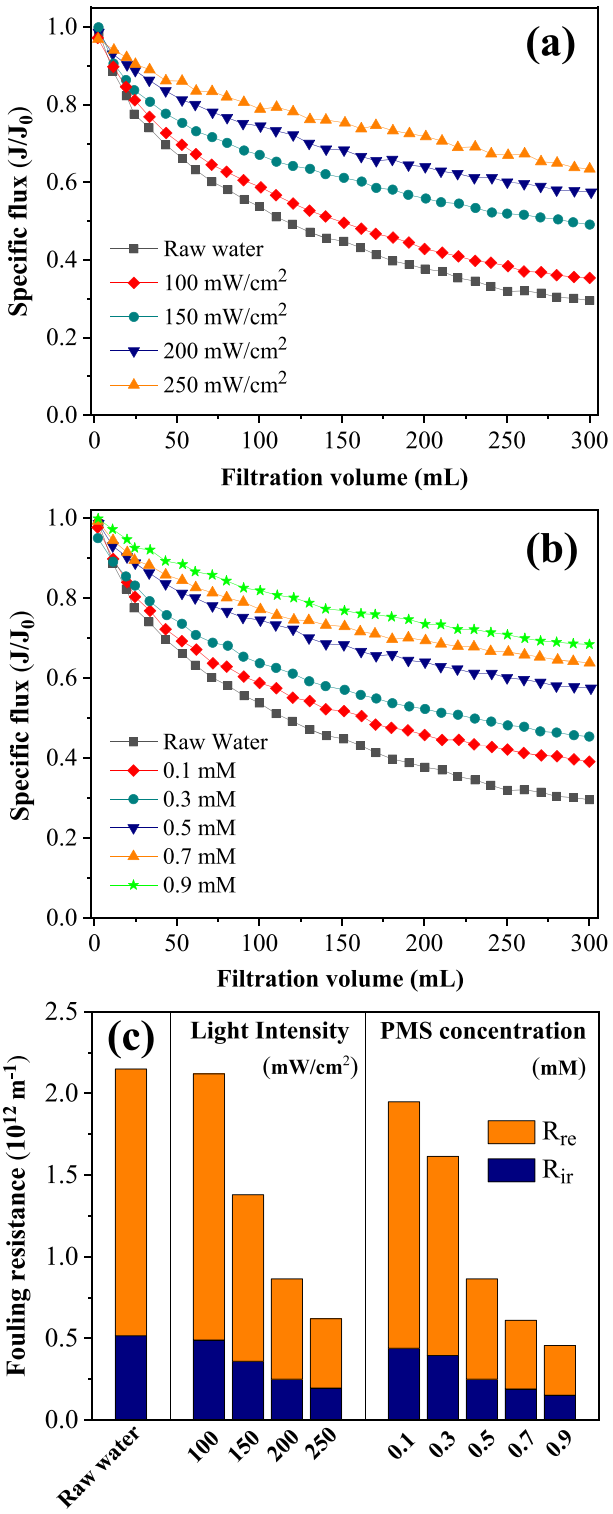

Fig. 3. Impacts of the pretreatment on membrane flux (a, b) and reversibility (c) at different light intensities ($[PMS]_0$=0.5 mM) and PMS concentrations (light intensity=200 mW/cm^2).

sunlight-induced PMS activation could mitigate membrane fouling. The filtration flux of raw water severely declined, with a decrease of approximately 0.30 (J/J_0) of the initial flux. The final ultrafiltration flux rose from 0.35 to 0.63 with an increase of light intensity from 100 to 250 mW/cm^2 (Fig. 3a). The fluxes were improved by 17%, 66%, 94%, and 110%, respectively, in comparison with raw water filtration, implying that increase of light intensity alleviated membrane fouling, which corresponded with the removal and mineralization results of organic matter.

Fig. 3b showed the effect of PMS concentration on the flux of the ultrafiltration membrane when light intensity was 200 mW/cm^2. With the increase in PMS content from 0.1 to 0.9 mM, the fluxes of the ultrafiltration membrane were improved by 30% to 127%. In general, increasing the PMS amount could improve the membrane flux better. Nevertheless, ultrafiltration flux increased slowly when the PMS dosage exceeded 0.5 mM. It could be concluded that the simulated sunlight-induced PMS pretreatment had less effect on improving the membrane flux when PMS dosage was greater than 0.5 mM. This could be interpreted with the following two reasons. On the one hand, most of the organic matters, which could be excited by the simulated sunlight to activate PMS, were removed with the addition of 0.5 mM PMS (Fig. 1). On the other hand, a small amount of ultraviolet light, around 320–380 nm in the sunlight spectrum (Fig. S2), did not activate PMS effectively (Nie et al., 2022).

The effect of pretreatment on the reversibility of membrane fouling during the ultrafiltration process was shown in Fig. 3c. The reversible (R_r) and irreversible (R_{ir}) fouling resistances of filtration of raw water were 1.63 × 10^{12} and 0.52 × 10^{12} m^{-1}, respectively. Sunlight-induced PMS pretreatments effectively decreased the R_r and R_{ir} excepting the system irradiated by 100 mW/cm^2. Our 100 mW/cm^2 system had similar NOM removal compared with the results by Guo et al. (2021). However, it was inconsistent with controlling the fouling resistances (resistances reduced in his system), which might be ascribed to the difference in filtration condition. With light intensity rising from 150 to 250 mW/cm^2, the R_{ir} decreased from 0.36 × 10^{12} to 0.20 × 10^{12} m^{-1}, which were 30.7% to 61.5% lower than that of filtration of raw water. When the PMS dosage increased from 0.1 to 0.9 mM, the R_{ir} decreased by 14.7% to 70.5%, compared to raw water. Accordingly, the R_r reduced by 37.6% to 73.9% from 150 to 250 mW/cm^2 and 7.6% to 81.4% from 0.1 to 0.9 mM. The decreases in fouling resistances were consistent with NOM removals. Furthermore, the proportions of R_r to R_{ir} decreased with the light intensity and PMS dosage, indicating that the contribution of sunlight-induced PMS pretreatment to alleviate reversible fouling was better than irreversible fouling. From the actual needs of balancing water quality, membrane flux (fouling resistance), and economy, using 200 mW/cm^2 (2-sun) irradiation and adding 0.5 mM PMS were the optimal conditions for removing organic substances and mitigating membrane fouling.

3.3. *Membrane fouling prediction*

The NOM contributed primarily to the membrane fouling during the ultrafiltration of surface water. To better predict and control membrane fouling, the correlations between various NOM indicators (UV_{254}, DOC, and F_{max} of fluorescent component) and membrane fouling indices (TFI and HIFI) were established, as shown in Fig. 4. UV_{254} had strong positive correlations with both TFI and HIFI, and the R^2 were 0.7949 (P = 0.0012) and 0.7875 (P = 0.0014), respectively (Fig. 4a). DOC showed moderate positive correlations with TFI (R^2=0.5822, P = 0.0168) and HIFI (R^2=0.4738, P = 0.0404) (Fig. 4b). UV_{254} had apparent influences on the total fouling and irreversible fouling of the ultrafiltration membrane, while DOC exhibited limited influences. Similar results were also found in sunlight(100 mW/cm^2)-heat/PDS pretreatment system by Guo et al. (2021). Furthermore, Cheng et al. (2016) used pre-ozonation for the Songhua River water before ultrafiltration and found no significant correlations between DOC and both fouling indices (TFI and HIFI), but much rather the UV_{254}. Low-dosage pre-ozonation only transformed high MW components in NOM into small MW fragments (rather than into CO_2 and H_2O), which were more likely to pass through membrane pores, resulting in an increase of DOC in membrane effluent (Cheng et al., 2016). In terms of control of ultrafiltration membrane fouling, the effective removal of UV_{254} could be considered as a key indicator (Guo et al., 2021). However, to meet the quality of membrane effluent, it is

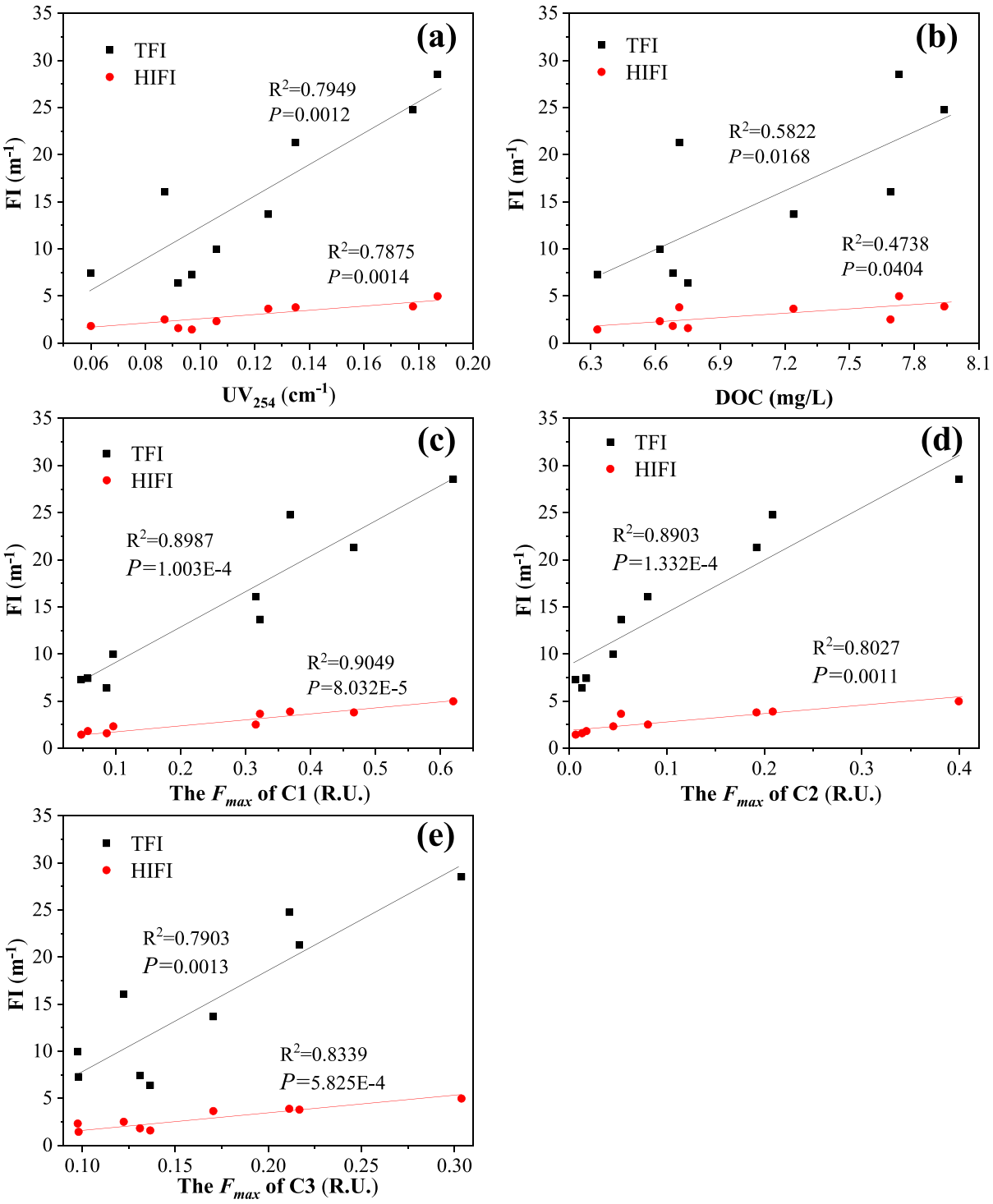

Fig. 4. Correlations between fouling indices (TFI and HIFI) with UV_{254} (a), DOC (b), F_{max} of C1 (c), C2 (d), and C3 (e). The R^2 value is the correlation coefficient, and the *P* value represents the significance level between fouling indices and water quality parameters.

recommended to consider DOC removal. Although removal of DOC in our system was not as high as in other systems, DOC of ultrafiltration effluent was effectively controlled. All the F_{maxs} of C1, C2 and C3 components were highly correlated with TFI (R^2=0.8987, 0.8903, and 0.7903, respectively) and HIFI (R^2=0.9049, 0.8027 and 0.8339, respectively) (Fig. 4c–e). By comparison, both C1 and C2 had the best correlations with TFI, indicating that humic-like matter mainly contributed to the total membrane fouling. Moreover, C1 showed a higher correlation with HIFI compared to C2. Based on the previous study (Lee et al., 2015), for humic matter, fluorescence peaks at longer emission wavelengths usually exhibited a more cohesive structure and higher MW. Hence, C1 with a smaller MW was more likely to cause irreversible fouling than C2. The protein-like substance, C3, was also the main contaminant that caused irreversible membrane fouling. However, due to its very low content in Songhua River water, the contribution to irreversible membrane fouling was inferior to C1. In a word, the UV_{254} and the F_{maxs} of C1, C2, and C3 components were key indicators to predict and control membrane fouling.

3.4. Mechanism of membrane fouling control

3.4.1. Mathematical modeling for membrane fouling process

The J/J_0 curves were fitted with the four classic filtration models to interpret the membrane fouling process, and the results were displayed in Table 1. The correlation coefficient (R^2) of raw water filtration fitted by complete blocking, standard blocking, intermediate blocking, and cake filtration models were 0.8603, 0.9960, 0.9448, and 0.9923, respectively, indicating that there were multiple fouling mechanisms caused by raw water, and standard blocking and cake filtration dominated membrane fouling. The sunlight-induced PMS pretreatment changed the membrane fouling process. With the increase of light intensity and PMS dosage, the correlation coefficient (R^2) of both standard blocking and cake filtration models decreased slightly while it increased significantly for complete blocking (from 0.8603 to 0.9634 and 0.9371). Moreover, the correlation coefficient (R^2) of intermediate blocking did not change significantly. The proportions of standard blocking and cake filtration in the membrane fouling were reduced, but complete blocking increased. These implied that the internal fouling of membrane pores and cake layer fouling were alleviated, which was beneficial to reducing membrane fouling resistance and improving membrane flux. The sunlight-induced PMS pretreatment could degrade high MW organics into low MW compounds and mineralize some low MW fractions to control standard blocking and cake filtration fouling (Xing et al., 2018), which was supported by NOM removal results and following HPSEC chromatograms. However, some degraded low MW compounds were retained on the membrane pores, which contributed to complete blocking (Xing et al., 2018).

3.4.2. NOM MW variation and generation of active species

The MW distributions of NOM by pretreatment were detected with HPSEC (Fig. 5a). HPSEC chromatogram of raw water contained two significant peaks (Peak A, MW distributed in the range of 5-23 kDa with a peak value at 8.2 kDa and Peak C in the range of 250–1100 Da with a peak value at 650 Da) and one minor peak (Peak B in the range of 2.2–5 kDa with a peak value at 3.1 kDa). According to the research by Brezinski and Gorczyca (2019), Peak A and peak B belong to the humics, and peak C was assigned to the low MW acids, humics, and/or building blocks. Ultrafiltration alone removed the minor peak B of raw water while decreasing the intensity of peak A and peak C slightly. The size of membrane pore (100 kDa) exceeded the size of NOM in the Songhua River water, thus leading to the limited interception of pollutants by ultrafiltration alone. Compared with raw water, MW distributions of water samples by the pretreatment and pretreatment/ultrafiltration were changed. Peak A disappeared, and a new and stronger peak D in the low MW range of 1.1–13.6 kDa appeared with a peak value at 6.5 kDa.

Table 1
R^2 values of regression analyses for membrane fouling of different systems.

Pretreatments	Membrane fouling models			
Light intensity (mW/cm^2)	Complete blocking	Standard blocking	Intermediate blocking	Cake filtration
Direct ultrafiltration	0.8603	0.9960	0.9448	0.9923
100	0.8879	0.9886	0.9568	0.9903
150	0.8940	0.9891	0.9469	0.9808
200	0.9256	0.9828	0.9589	0.9820
250	0.9634	0.9910	0.9802	0.9895
PMS concentration (mM)				
Direct ultrafiltration	0.8603	0.9960	0.9448	0.9923
0.1	0.8750	0.9932	0.9445	0.9856
0.3	0.9036	0.9880	0.9540	0.9859
0.5	0.9256	0.9828	0.9589	0.9820
0.7	0.9120	0.9935	0.9422	0.9660
0.9	0.9371	0.9827	0.9593	0.9766

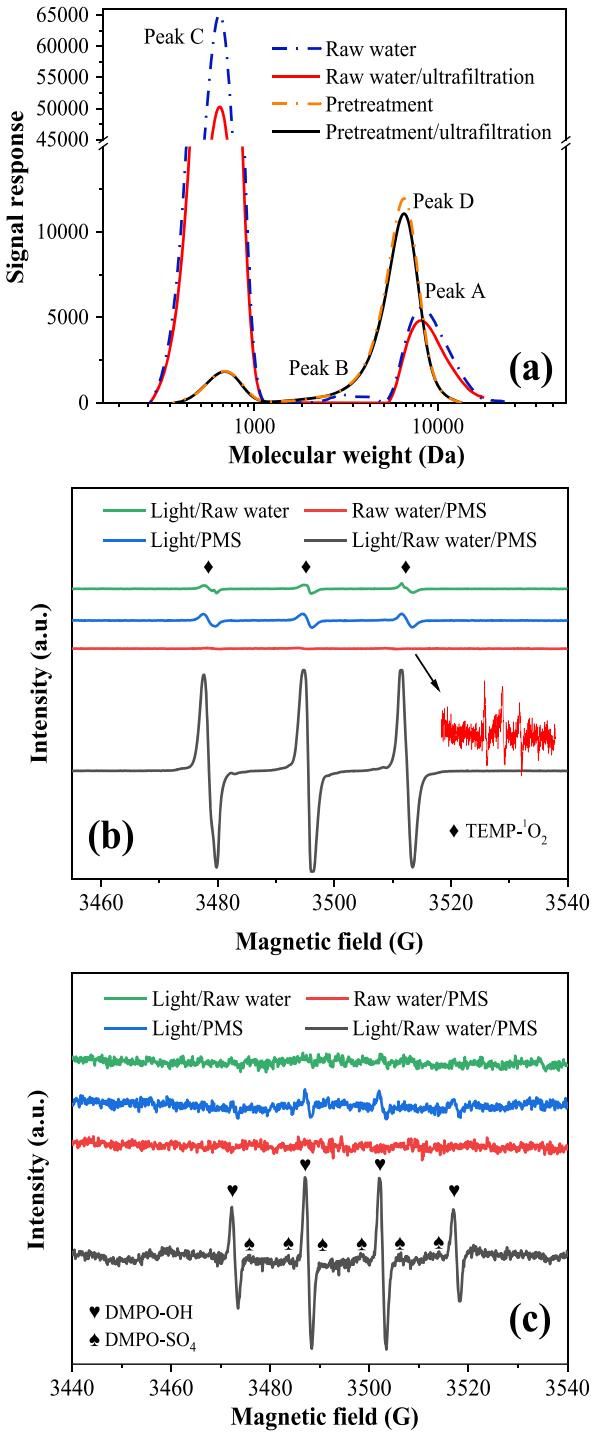

Fig. 5. MW distributions of the water samples (a) and ESR spectra obtained from the different systems in the presence of TEMP (b) and DMPO (c) (◆ represents $^1O_2$ adduct, ♥ represents •OH adduct, ♠ represents SO_4•$^-$ adduct). The pretreatment conditions: $[PMS]_0$=0.5 mM, light intensity=200 mW/cm^2, $[TEMP]_0$=20 mM, $[DMPO]_0$=50 mM.

This was ascribed to the degradation of large MW humics into small ones. The intensity of peak C was markedly decreased after the pretreatment, indicating that some low MW substances were mineralized. There was no difference in the intensity of peak C between pretreatment and pretreatment/ultrafiltration, while the intensity of peak D was decreased after pretreatment/ultrafiltration. This indicated that the probability of membrane interception was positively correlated with the concentration of organic substances (Guo et al., 2020), and low

concentration of low MW substances could directly pass through the membrane pores. Overall, the pretreatment reduced low MW NOM in ultrafiltration effluent effectively.

To explore the mechanism of NOM removal, active species derived from the photoinduced activation of PMS in raw water were identified by ESR with 5,5-dimethyl-1-pyrolin-N-oxide (DMPO) and 2,2,6,6-tetramethyl-4-piperidinol (TEMP) as spin-trapping agents (Fig. 5b and c). Fig. 5b showed that adding PMS into raw water generated very few $^1O_2$ without illumination. It is related to the reaction of NOM in the river water with PMS (Zhou et al., 2017). The direct photolysis of PMS can form $^1O_2$ due to the dismutation reaction of $SO_5^{\bullet-}$ (Huie et al., 1989). Meanwhile, the signals of •OH were also observed (Fig. 5c). In the irradiated raw water system, the ^{3}NOM* generated by light-induced NOM can react with dissolved oxygen to produce $^1O_2$ (Nie et al., 2022). Additionally, all the •OH, $SO_4^{\bullet-}$, and $^1O_2$ were found in the irradiated raw water/PMS system. Apparently, these signals were significantly greater than the sums of the signals from the direct photolysis of PMS, the irradiated raw water and the raw water/PMS systems. This result confirmed that the photo-induced NOM could trigger PMS activation to yield a substantial amount of active species, which were involved in the degradation of NOM. The humics with MW distribution of 5–23 kDa in river water (Fig. 5a) contained abundant aromatic constituents/phenolic groups and quinone groups (Jia et al., 2020), which owned the electron-donating and electron-transferring capacity, respectively (Aeschbacher et al., 2011; Roden et al., 2010). Under sunlight irradiation, NOM with aromatic constituents/phenolic groups could be induced to form hydrated electrons (e_{aq}^-) and excited state NOM (^{3}NOM*). The hydrated electrons were transferred via the quinone groups of NOM to activate PMS, resulting in the generation of $SO_4^{\bullet-}$ and •OH. Meanwhile, PMS reacted with ^{3}NOM* to form $SO_4^{\bullet-}$ or $SO_5^{\bullet-}$, while the latter was responsible for the generation of $^1O_2$ (Jia et al., 2020; Nie et al., 2022).

3.4.3. Ultrafiltration membrane characterization

A series of characterizations were performed to prove the alleviation of membrane fouling. The functional groups of the membrane surface were identified with FTIR (Fig. 6). The absorption peaks at 1075 and 1107 cm^{-1} corresponded to the aromatic ring vibrations in the polyethersulfone membrane (Guo et al., 2020; Wang et al., 2015). The 1150 cm^{-1} and 1297/1322 cm^{-1} doublet resulted from the symmetric and antisymmetric O=S=O stretching vibrations of the sulfone group, respectively (Guo et al., 2020; Wang et al., 2015). Three other strong absorption peaks around 915, 1031, and 3380 cm^{-1} were found in the fouled membrane. The broad peak around 3380 cm^{-1} was associated with the stretching vibration of O-H bonds (Li et al., 2016). The peaks at 915 and 1031 cm^{-1} were assigned to Si-O or C-O-C bonds, which were likely to be the silicon precipitate or organic substances in the Songhua River water (Gamage and Chellam, 2014; Guo et al., 2020). The fouling peak intensities decreased obviously with the pretreatment, and the FTIR spectrum of the membrane fouled by the pretreated water was more similar to that of the virgin membrane relative to the membrane fouled by raw water. Sunlight induced NOM/PMS pretreatment could reduce the intercepted pollutants on the membrane surface.

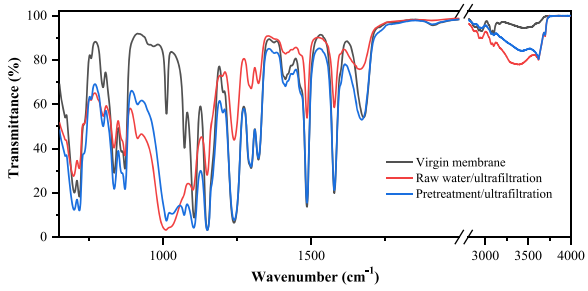

Fig. 6. FTIR spectra of membranes. The pretreatment conditions: $[PMS]_0$=0.5 mM, light intensity=200 mW/cm^2.

Fig. 7a–c exhibited the surface morphology of virgin and fouled membranes. The surface of the virgin membrane was clean and smooth, and membrane pores were evenly distributed. After filtration of raw water, the membrane surface was covered with a dense and large nubby fouling layer, which blocked membrane pores completely. The membrane pores which were filtrated with pretreated water, were still blocked completely. Nevertheless, the size of the foulants slightly decreased, and more gaps could be discerned on the fouling layer. In the cross-sectional images of the fouled membranes, a fouling/cake layer with a thickness of approximately 0.74 μm could be observed on the ultrafiltration membrane after filtration of raw water. A thin fouling/cake layer (0.35 μm) appeared on the membrane surface when raw water was treated by the simulated sunlight/PMS pre-oxidation. Further, EDX characterization detected fourteen elements on the fouled membranes, including C, O, S, Na, Mg, Al, Si, P, N, Cl, K, Ca, Mn, and Fe, as shown in Fig. S6. Variations of C, O, and N elements indicated that organic fouling occurred during the ultrafiltration process. In addition, inorganic precipitation also appeared on the membrane surface. After the pretreatment, the organic fouling and inorganic precipitation were obviously reduced. Previous studies had reported that metal cations, like Ca^{2+}, could bond humic acid molecules via a bridging effect to generate larger molecules that promoted the formation of membrane fouling (Li et al., 2020; Tian et al., 2013; Wang et al., 2015). Additionally, K^+ would induce the electrostatic shielding effect to compress humic acid molecules, resulting in the aggravation of recalcitrant irreversible fouling (Li et al., 2020). The HPSEC results showed that humics was the main component of NOM in the Songhua River water. The sunlight-induced NOM/PMS pretreatment could play the de-complexation effect by destroying the structure of humics and inhibiting the linking of metal cations to humics, hence reducing the deposition of metal cations on the membrane surface.

AFM images showed the surface roughness and topography of membranes (Fig. 7d). The bright areas/peaks and dark areas/valleys on the surface of the virgin membrane were evenly distributed. In contrast, the size of bright and dark areas and the distribution of peaks and valleys of the used membranes had been changed significantly, implying that foulants covered membrane surface. Obviously, the fluctuation/change of peaks and valleys on the membrane fouled by raw water exceeded that of the membrane fouled by pretreated water, which further supported the size of the pollutants observed by the SEM. Because of the interception of the large molecules of humic acid, the metal cations linked humic acid, and the inorganic precipitate, membrane filtration of raw water exhibited a rough and uneven surface with a surface roughness of Rq=52.8 nm, which was higher than that of membrane fouled by pretreated water (Rq = 26.4 nm) and virgin membrane (Rq = 12.2 nm). After the destruction of high MW substances, the mineralization of low MW fractions, and the de-complexation effect by sunlight induced NOM/PMS pre-oxidation, less NOM and inorganic components were retained on the membrane surface, resulting in a very thin cake/fouling layer and a low surface roughness. The results verified that sunlight-induced NOM/PMS pretreatment not only controlled the organic fouling of the ultrafiltration membrane but also reduced its inorganic fouling remarkably.

4. Conclusions

In summary, the photo-induced activation of PMS in sunlit NOM-contained natural surface water was conducted as pretreatment before ultrafiltration to remove NOM and control membrane fouling. With increased light intensity (100–250 mW/cm^2) and PMS dosage (0.1–0.9 mM), the pretreatment enabled to remove NOM in the Songhua River water, decrease membrane fouling and improve water flux effectively. The conditions of 200 mW/cm^2/0.5 mM PMS removed 57.5%, 18.5%, 84–94%, and 60% for UV_{254}, DOC, humic-like substance, and protein-like component, respectively. Furthermore, the pretreatment improved

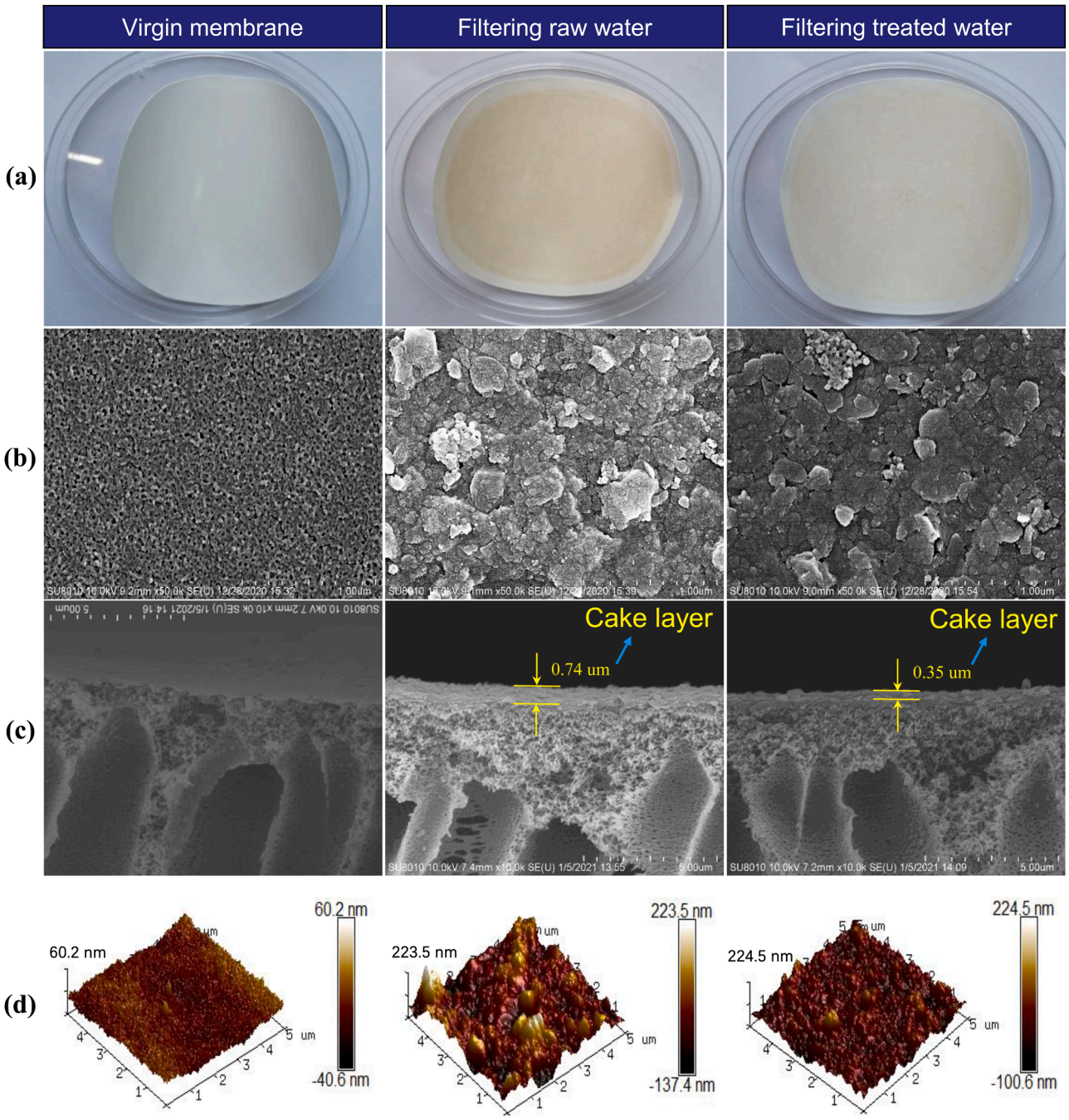

Fig. 7. Photographs (a), top-view SEM images (b), cross-sectional SEM images (c), and AFM images (d) of the membranes. The pretreatment conditions: $[PMS]_0$=0.5 mM, light intensity=200 mW/cm^2.

water flux by 94% and reduced R_r and R_{ir} by 62.4% and 51.9%, respectively. The UV_{254} and the F_{maxs} of three fluorescence components could be used as key indexes to predict and control membrane fouling due to their significant correlations with TFI and HIFI. The pretreatment alleviated the dominant standard blocking and cake layer blocking. The simulated sunlight-induced NOM (^{3}NOM* and e_{aq}^-) were capable of activating PMS to produce $SO_4^{\bullet-}$, •OH, and $^1O_2$. They destroyed high MW organics, mineralized low MW compounds, and hindered organics linking with inorganic cations, thereby reducing both organic and inorganic membrane fouling, which showed a thin cake layer and a low surface roughness. This study provides new insights for coupling solar energy and membrane filtration in water treatment. It raises the question that the simulated sunlight resource consumes electric energy. Based on our research, we will endeavor to further develop a decentralized potable water treatment device by using a sunlight-focusing reactor in an actual environment instead of the simulated sunlight (Lin et al., 2019).

Declaration of Competing Interest

The authors declare that they have no known competing financial interests or personal relationships that could have appeared to influence the work reported in this paper.

Data availability

No data was used for the research described in the article.

Acknowledgments

This work was financially supported by the Startup Foundation for Introducing Talent of Nanjing University of Information Science and Technology, Postgraduate Research & Practice Innovation Program of Jiangsu Province (No. SJCX22_0370), Heilongjiang Touyan Innovation Team Program (No. HIT-SE-01), National Natural Science Foundation of China (No. 51961125104), and Medicine, Engineering and Science Cross Fund of Harbin Institute of Technology (No. IR2021107).

Supplementary materials

Supplementary material associated with this article can be found, in the online version, at doi:10.1016/j.watres.2022.119452.

References

Aeschbacher, M., Vergari, D., Schwarzenbach, R.P., Sander, M., 2011. Electrochemical analysis of proton and electron transfer equilibria of the reducible moieties in humic acids. Environ. Sci. Technol. 45 (19), 8385–8394.

Brezinski, K., Gorczyca, B., 2019. An overview of the uses of high performance size exclusion chromatography (HPSEC) in the characterization of natural organic matter (NOM) in potable water, and ion-exchange applications. Chemosphere 217, 122–139.

Chen, Y., Hu, C., Hu, X., Qu, J., 2009. Indirect photodegradation of amine drugs in aqueous solution under simulated sunlight. Environ. Sci. Technol. 43 (8), 2760–2765.

Chen, Z., Li, M., Wen, Q., Ren, N., 2017. Evolution of molecular weight and fluorescence of effluent organic matter (EfOM) during oxidation processes revealed by advanced spectrographic and chromatographic tools. Water Res. 124, 566–575.

Cheng, X., Liang, H., Ding, A., Qu, F., Shao, S., Liu, B., Wang, H., Wu, D., Li, G., 2016. Effects of pre-ozonation on the ultrafiltration of different natural organic matter (NOM) fractions: membrane fouling mitigation, prediction and mechanism. J. Membr. Sci. 505, 15–25.

Cheng, X., Liang, H., Ding, A., Tang, X., Liu, B., Zhu, X., Gan, Z., Wu, D., Li, G., 2017a. Ferrous iron/peroxymonosulfate oxidation as a pretreatment for ceramic ultrafiltration membrane: control of natural organic matter fouling and degradation of atrazine. Water Res. 113, 32–41.

Cheng, X., Liang, H., Ding, A., Zhu, X., Tang, X., Gan, Z., Xing, J., Wu, D., Li, G., 2017b. Application of Fe(II)/peroxymonosulfate for improving ultrafiltration membrane performance in surface water treatment: comparison with coagulation and ozonation. Water Res. 124, 298–307.

Cheng, X., Wu, D., Liang, H., Zhu, X., Tang, X., Gan, Z., Xing, J., Luo, X., Li, G., 2018. Effect of sulfate radical-based oxidation pretreatments for mitigating ceramic UF membrane fouling caused by algal extracellular organic matter. Water Res. 145, 39–49.

Gamage, N.P., Chellam, S., 2014. Mechanisms of physically irreversible fouling during surface water microfiltration and mitigation by aluminum electroflotation pretreatment. Environ. Sci. Technol. 48 (2), 1148–1157.

Gao, W., Liang, H., Ma, J., Han, M., Chen, Z.L., Han, Z.S., Li, G.B., 2011. Membrane fouling control in ultrafiltration technology for drinking water production: a review. Desalination 272 (1), 1–8.

Gao, Y., Zhu, Y., Lyu, L., Zeng, Q., Xing, X., Hu, C., 2018. Electronic structure modulation of graphitic carbon nitride by oxygen doping for enhanced catalytic degradation of organic pollutants through peroxymonosulfate activation. Environ. Sci. Technol. 52 (24), 14371–14380.

Guo, Y., Liang, H., Bai, L., Huang, K., Xie, B., Xu, D., Wang, J., Li, G., Tang, X., 2020. Application of heat-activated peroxydisulfate pre-oxidation for degrading contaminants and mitigating ultrafiltration membrane fouling in the natural surface water treatment. Water Res. 179, 115905.

Guo, Y., Liang, H., Li, G., Xu, D., Yan, Z., Chen, R., Zhao, J., Tang, X., 2021. A solar photo-thermochemical hybrid system using peroxydisulfate for organic matters removal and improving ultrafiltration membrane performance in surface water treatment. Water Res. 188, 116482.

Howe, K.J., Clark, M.M., 2002. Fouling of microfiltration and ultrafiltration membranes by natural waters. Environ. Sci. Technol. 36 (16), 3571–3576.

Huie, R.E., Clifton, C.L., Altstein, N., 1989. A pulse radiolysis and flash photolysis study of the radicals SO-2, SO-3, SO-4 and SO-5. Int. J. Radiat. Appl. Instrum. Part C 33 (4), 361–370.

Jia, J., Liu, D., Tian, J., Wang, W., Ni, J., Wang, X., 2020. Visible-light-excited humic acid for peroxymonosulfate activation to degrade bisphenol A. Chem. Eng. J. 400, 125853.

Lee, B.M., Seo, Y.S., Hur, J., 2015. Investigation of adsorptive fractionation of humic acid on graphene oxide using fluorescence EEM-PARAFAC. Water Res. 73, 242–251.

Lee, N., Amy, G., Croué, J.P., Buisson, H., 2004. Identification and understanding of fouling in low-pressure membrane (MF/UF) filtration by natural organic matter (NOM). Water Res. 38 (20), 4511–4523.

Li, B., He, X., Wang, P., Liu, Q., Qiu, W., Ma, J., 2020. Opposite impacts of K^+ and Ca^{2+} on membrane fouling by humic acid and cleaning process: Evaluation and mechanism investigation. Water Res. 183, 116006.

Li, D., Jia, J., Zhang, Y., Wang, N., Guo, X., Yu, X., 2016. Preparation and characterization of Nano-graphite/TiO2 composite photoelectrode for photoelectrocatalytic degradation of hazardous pollutant. J. Hazard. Mater. 315, 1–10.

Lin, T., Pan, S., Chen, W., Bin, S., 2013. Role of pre-oxidation, using potassium permanganate, for mitigating membrane fouling by natural organic matter in an ultrafiltration system. Chem. Eng. J. 223, 487–496.

Lin, Y.C., Panchangam, S.C., Liu, L.C., Lin, A.Y.C., 2019. The design of a sunlight-focusing and solar tracking system: a potential application for the degradation of pharmaceuticals in water. Chemosphere 214, 452–461.

Ma, B., Qi, J., Wang, X., Ma, M., Miao, S., Li, W., Liu, R., Liu, H., Qu, J., 2018. Moderate KMnO4-Fe(II) pre-oxidation for alleviating ultrafiltration membrane fouling by algae during drinking water treatment. Water Res. 142, 96–104.

Nie, J., Zou, J., Yan, S., Song, W., 2022. Photosensitized transformation of peroxymonosulfate in dissolved organic matter solutions under simulated solar irradiation. Environ. Sci. Technol. 56 (3), 1963–1972.

Pan, Y., Garg, S., Waite, T.D., Yang, X., 2018. Copper inhibition of triplet-induced reactions involving natural organic matter. Environ. Sci. Technol. 52 (5), 2742–2750.

Peter-Varbanets, M., Zurbrügg, C., Swartz, C., Pronk, W., 2009. Decentralized systems for potable water and the potential of membrane technology. Water Res. 43 (2), 245–265.

Peters, C.D., Rantissi, T., Gitis, V., Hankins, N.P., 2021. Retention of natural organic matter by ultrafiltration and the mitigation of membrane fouling through pre-treatment, membrane enhancement, and cleaning - a review. J. Water Process Eng. 44, 102374.

Prézélus, F., Tiruta-Barna, L., Remigy, J.C., Guigui, C., 2021. Process-based LCA of ultrafiltration for drinking water production. Water Res. 199, 117156.

Roden, E.E., Kappler, A., Bauer, I., Jiang, J., Paul, A., Stoesser, R., Konishi, H., Xu, H., 2010. Extracellular electron transfer through microbial reduction of solid-phase humic substances. Nat. Geosci. 3 (6), 417–421.

Shao, S., Feng, Y., Yu, H., Li, J., Li, G., Liang, H., 2017. Presence of an adsorbent cake layer improves the performance of gravity-driven membrane (GDM) filtration system. Water Res. 108, 240–249.

Shao, S., Liang, H., Qu, F., Yu, H., Li, K., Li, G., 2014. Fluorescent natural organic matter fractions responsible for ultrafiltration membrane fouling: identification by adsorption pretreatment coupled with parallel factor analysis of excitation–emission matrices. J. Membr. Sci. 464, 33–42.

Stedmon, C.A., Bro, R., 2008. Characterizing dissolved organic matter fluorescence with parallel factor analysis: a tutorial. Limnol. Oceanogr. Methods 6 (11), 572–579.

Tian, D., Zhou, H., Zhang, H., Zhou, P., You, J., Yao, G., Pan, Z., Liu, Y., Lai, B., 2022. Heterogeneous photocatalyst-driven persulfate activation process under visible light irradiation: from basic catalyst design principles to novel enhancement strategies. Chem. Eng. J. 428, 131166.

Tian, J.Y., Ernst, M., Cui, F., Jekel, M., 2013. Effect of different cations on UF membrane fouling by NOM fractions. Chem. Eng. J. 223, 547–555.

Tian, J., Wu, C., Yu, H., Gao, S., Li, G., Cui, F., Qu, F., 2018. Applying ultraviolet/persulfate (UV/PS) pre-oxidation for controlling ultrafiltration membrane fouling by natural organic matter (NOM) in surface water. Water Res. 132, 190–199.

Tian, J., Yu, H., Shen, Y., Shi, W., Liu, D., Gao, S., Cui, F., 2016. Identification of irreversible UF membrane foulants by fluorescence excitation–emission matrix coupled with parallel factor analysis. Desalin. Water Treat. 57 (46), 21794–21805.

Wan, Y., Xie, P., Wang, Z., Ding, J., Wang, J., Wang, S., Wiesner, M.R., 2019. Comparative study on the pretreatment of algae-laden water by UV/persulfate, UV/chlorine, and UV/H2O2: variation of characteristics and alleviation of ultrafiltration membrane fouling. Water Res. 158, 213–226.

Wang, L.F., He, D.Q., Chen, W., Yu, H.Q., 2015. Probing the roles of Ca^{2+} and Mg^{2+} in humic acids-induced ultrafiltration membrane fouling using an integrated approach. Water Res. 81, 325–332.

Wang, X., Sun, M., Zhao, Y., Wang, C., Ma, W., Wong, M.S., Elimelech, M., 2020. *In situ* electrochemical generation of reactive chlorine species for efficient ultrafiltration membrane self-cleaning. Environ. Sci. Technol. 54 (11), 6997–7007.

Wang, X., Wang, S., Qu, R., Ge, J., Wang, Z., Gu, C., 2018. Enhanced removal of chlorophene and 17β-estradiol by Mn(III) in a mixture solution with humic acid: investigation of reaction kinetics and formation of co-oligomerization products. Environ. Sci. Technol. 52 (22), 13222–13230.

Wells, M.J.M., Hooper, J., Mullins, G.A., Bell, K.Y., 2022. Development of a fluorescence EEM-PARAFAC model for potable water reuse monitoring: Implications for inter-component protein–fulvic–humic interactions. Sci. Total Environ. 820, 153070.

Wu, S., Hua, X., Ma, B., Fan, H., Miao, R., Ulbricht, M., Hu, C., Qu, J., 2021. Three-dimensional analysis of the natural-organic-matter distribution in the cake layer to precisely reveal ultrafiltration fouling mechanisms. Environ. Sci. Technol. 55 (8), 5442–5452.

Xing, J., Wang, H., Cheng, X., Tang, X., Luo, X., Wang, J., Wang, T., Li, G., Liang, H., 2018. Application of low-dosage UV/chlorine pre-oxidation for mitigating ultrafiltration (UF) membrane fouling in natural surface water treatment. Chem. Eng. J. 344, 62–70.

Yang, Y., Jiang, J., Lu, X., Ma, J., Liu, Y., 2015. Production of sulfate radical and hydroxyl radical by reaction of ozone with peroxymonosulfate: a novel advanced oxidation process. Environ. Sci. Technol. 49 (12), 7330–7339.

Yu, H., Li, X., Chang, H., Zhou, Z., Zhang, T., Yang, Y., Li, G., Ji, H., Cai, C., Liang, H., 2020. Performance of hollow fiber ultrafiltration membrane in a full-scale drinking water treatment plant in China: a systematic evaluation during 7-year operation. J. Membr. Sci. 613, 118469.

Yu, W., Graham, N.J.D., 2015. Application of Fe(II)/K2MnO4 as a pre-treatment for controlling UF membrane fouling in drinking water treatment. J. Membr. Sci. 473, 283–291.

Zhang, D., Yan, S., Song, W., 2014. Photochemically Induced formation of Reactive Oxygen Species (ROS) from effluent organic matter. Environ. Sci. Technol. 48 (21), 12645–12653.

Zhao, Y., Lu, D., Cao, Y., Luo, S., Zhao, Q., Yang, M., Xu, C., Ma, J., 2018. Interaction analysis between gravity-driven ceramic membrane and smaller organic matter: implications for retention and fouling mechanism in ultralow pressure-driven filtration system. Environ. Sci. Technol. 52 (23), 13718–13727.

Zhou, Y., Jiang, J., Gao, Y., Pang, S.Y., Yang, Y., Ma, J., Gu, J., Li, J., Wang, Z., Wang, L. H., Yuan, L.P., Yang, Y., 2017. Activation of peroxymonosulfate by phenols: important role of quinone intermediates and involvement of singlet oxygen. Water Res. 125, 209–218.

Zularisam, A.W., Ismail, A.F., Salim, M.R., Sakinah, M., Ozaki, H., 2007. The effects of natural organic matter (NOM) fractions on fouling characteristics and flux recovery of ultrafiltration membranes. Desalination 212 (1), 191–208.